Quantitative analysis of the gain in probability of escaping for ideal phototactic swimmers due to chaotic dynamics

Alfredo J. Grados and Rafael D. Vilela*
Centro de Matemática, Computação e Cognição, UFABC, Santo André, SP, Brazil

(Received 29 January 2020; accepted 15 April 2020; published 27 May 2020)

We study the dynamics of ideal phototactic swimmers in a steady two-dimensional model flow with transport barriers. We consider a distant light source, in which case the self-propulsion velocity of the swimmers is, at any instant, along a predetermined direction. The probability of transport along that direction emerges from the competing effects of the swimmers' self-propulsion and the flow's transport barriers. For swimmers bounded to have the same time average self-propulsion speed, temporal modulation of that speed increases the probability of escaping due to the formation of a stochastic layer which fosters transport. We use separatrix-map techniques to calculate the gain in the probability of escaping.

DOI: 10.1103/PhysRevE.101.052617

I. INTRODUCTION

The interplay between fluid dynamics and the activity of transported material displays a plethora of complex phenomena which has motivated intense research [1]. In this context, a remarkable instance of activity of either biological or engineered nature corresponds to *self-propulsion* of the transported particles. These range from tiny organisms and nanoscaled manufactured swimmers in microchannels to the greatest mammals and large vessels in the ocean. As a result of the enormous range of possible Reynolds numbers involved, the underlying mechanisms and the emerging phenomena can be very distinct.

Small-scale swimming is dominated by viscosity and shows up in a number of different flavors, gyrotaxis, chemotaxis, and phototaxis being among the most common. Phototaxis, in particular, has been studied in unicellular organisms [2,3] and artificial microswimmers [4,5]. Both the dynamics of individual swimmers under a given flow and light stimulus [6] and the collective motion which emerges also from the interaction among swimmers [7] have been objects of research interest.

In this paper we study the phototactic dynamics of small individual swimmers far away from a light source in a steady fluid flow with transport barriers. We are interested in the nontrivial case where the self-propulsion velocity is small compared to the characteristic flow velocity. Transport or confinement is then the outcome of the delicate balance between self-propulsion along a fixed direction (that of the target source) and the flow's transport barriers. Our goal is to characterize the gain in the probability of *escaping*, i.e., overcoming such transport barriers, arising from a temporal modulation of the self-propulsion speed. More specifically, we compute and compare the probability of escaping of swimmers constrained to have a given self-propulsion mean speed but adopting two different *swimming strategies*. The first strategy corresponds to self-propulsion with constant speed and the second one corresponds to self-propulsion with a sinusoidal temporal modulation of the speed. For a given self-propulsion strategy, whether a certain individual swimmer will escape or remain trapped depends on its initial position, and the probability of escaping is defined by the relative measure of the set of initial conditions of trajectories which do not remain confined.

Generally speaking, we expect a gain in probability of escaping arising from a periodic modulation of the self-propulsion speed when the fluid flow is steady because such a modulation usually induces the formation of a stochastic layer (cf. Sec. IV A) which fosters transport. The intended contribution of the present work is to show that classical separatrix-map techniques can be a valuable yet simple tool for quantifying that probability gain in the context of phototaxis. It is worth noting that nearly periodic velocity oscillations of single swimming cells have been measured for unicellular algae [8] and that chaotic dynamics has been shown to result for gyrotactic microswimmers with temporal self-propulsion modulation [9].

II. PHOTOTAXIS AND FLUID FLOW MODEL

A. Model

A synthetic model for the motion of an individual *ideal* phototactic swimmer in a fluid flow is given by [6]

$$\dot{\mathbf{r}} = \mathbf{u}(\mathbf{r}, t) + \chi \nabla \Phi(\mathbf{r}), \tag{1}$$

where $\mathbf{u}(\mathbf{r}, t)$ is the velocity field of the fluid flow at the swimmer's position $\mathbf{r}$ and time t, and χ is the phototactic coefficient, which measures the strength of response of the swimmer to the illumination field $\Phi(\mathbf{r})$. The term $\chi \nabla \Phi(\mathbf{r})$ therefore describes phenomenologically the self-propulsion velocity of the swimmer.

We are interested in the case of a distant and localized light source, for which the phototactic term, $\chi \nabla \Phi(\mathbf{r})$, can be

*rafael.vilela@ufabc.edu.br

approximated by a constant self-propulsion velocity $\mathbf{v}_c$:

$$\dot{\mathbf{r}} = \mathbf{u}(\mathbf{r}, t) + \mathbf{v}_c, \tag{2}$$

which we shall refer to as the *first swimming strategy*.

Motivated in part by the growing interest in engineering microswimmers with different swimming properties, we pose the question whether a swimmer with no information whatsoever about the flow and bounded to have the same mean self-propulsion speed $\alpha \equiv |\mathbf{v}_c|$ as in the first strategy can increase its chance of escaping by modulating its speed. We thus introduce the *second swimming strategy* to be characterized in this paper:

$$\dot{\mathbf{r}} = \mathbf{u}(\mathbf{r}, t) + \mathbf{v}_c + \epsilon\ \sin(\Omega t)\hat{\mathbf{v}}_c, \tag{3}$$

where ϵ and Ω are, respectively, the amplitude and frequency of oscillations in the self-propulsion speed, and $\hat{\mathbf{v}}_c$ is the unit vector along the direction of $\mathbf{v}_c$.

For a specific flow field $\mathbf{u}(\mathbf{r}, t)$ we now describe, we shall compare the two swimming strategies above in their capacity to foster the transport of swimmers along $\hat{\mathbf{v}}_c$. For concreteness, we consider the classical planar cellular flow as a prototype for a steady flow with transport barriers. Incompressibility in dimension two allows us to write the fluid flow velocity field in terms of the stream function

$$\psi_f(x, y) = \sin(2\pi x)\sin(2\pi y). \tag{4}$$

The flow field is therefore given by $\mathbf{u}(\mathbf{r}, t) = (u_x, u_y) = (\partial_y\psi_f, -\partial_x\psi_f)$ and reads

$$\begin{aligned} u_x &= 2\pi\ \sin(2\pi x)\cos(2\pi y), \\ u_y &= -2\pi\ \cos(2\pi x)\sin(2\pi y). \end{aligned} \tag{5}$$

We point that the above fluid flow is prototypical for vortical flows which are attainable in microfluidic devices [10,11].

Assuming for simplicity that the constant self-propulsion velocity $\mathbf{v}_c$ is along the x axis, the first and second swimming strategies read

$$\begin{aligned} \frac{dx}{dt} &= 2\pi\ \sin(2\pi x)\cos(2\pi y) + \alpha + \epsilon\ \sin(\Omega t), \\ \frac{dy}{dt} &= -2\pi\ \cos(2\pi x)\sin(2\pi y), \end{aligned} \tag{6}$$

with $\epsilon = 0$ and $\epsilon \neq 0$, respectively. Note that the frequency Ω introduced by the second swimming strategy should be compared with some natural frequency Ω_0 defined by the flow field given by Eq. (5). To obtain Ω_0, we proceed as follows. The characteristic velocity U of the system can be taken as the root mean square of the fluid flow velocity (since α is comparatively small). We have $U = \sqrt{\int_0^1\int_0^1 (u_x^2 + u_y^2)dx\,dy} = \pi\sqrt{2}$. Now, the characteristic length L of the system is $1/2$, which is the size of a vortex cell. Therefore the characteristic frequency Ω_0 of the system is $\Omega_0 = 2\pi U/L = 4\pi^2\sqrt{2} \simeq 55.83$. This is a reference frequency with which Ω should be compared.

The phase portrait of Eq. (6) for $\epsilon = 0$ is shown in Fig. 1, where one can observe the coexistence of trapped and escaping trajectories. The first swimming strategy actually corresponds to a Hamiltonian system of one degree of freedom, with an *effective stream function* given by

$$\psi_0(x, y) = \psi_f(x, y) + \alpha y. \tag{7}$$

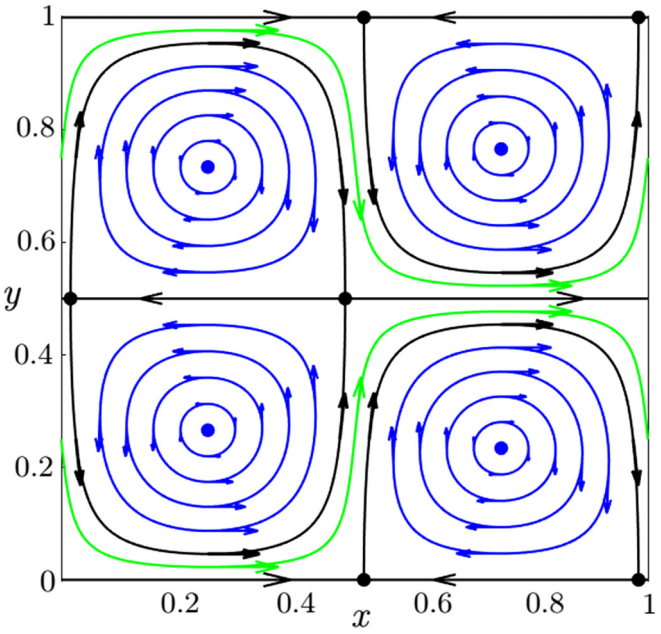

FIG. 1. Phase portrait of Eq. (6) with $\epsilon = 0$. The other parameter is $\alpha = \frac{\pi}{5}$. Both confined (blue) and escaping (green) trajectories are shown, as well the solutions separating them (black).

Chaos is expected in the region of the separatrices when a Hamiltonian system of one degree of freedom is subject to a nonautonomous perturbation. This is indeed visible in a Poincaré section for solutions of Eq. (6) in the case $\epsilon \neq 0$, shown in Fig. 2. Chaos produces transport between confined and nonconfined regions. In order to compare the strategies (Sec. V) in their efficiency to foster transport, we first derive expressions for the area of the set of initial conditions of escaping trajectories for vanishing and finite ϵ, respectively, in Secs. III and IV. Before that, let us discuss the validity and limitations of our model.

B. Validity and limitations of the model

Equation (1) is a phenomenological model that neglects the finite size of the swimmers. Real phototactic swimmers are finite-size particles with a density that can differ from that of the background fluid. In the biological context, both swimmer

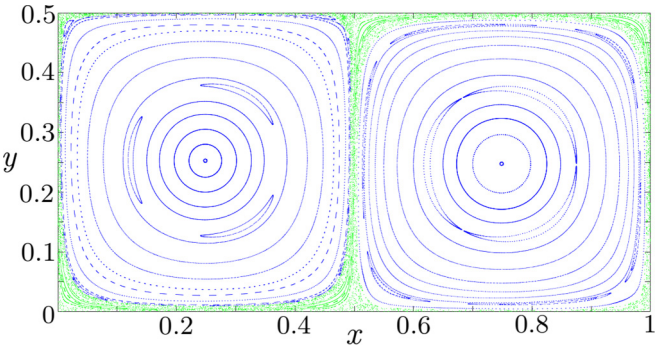

FIG. 2. Poincaré section for solutions of Eq. (6) with finite ϵ. The parameters are $\alpha = \frac{\pi}{5}$, $\epsilon = 0.3$, and $\Omega = 75$. Escaping trajectories are shown in green.

and background fluid have water as a major component. Therefore it is reasonable to treat biological swimmers as neutrally buoyant finite-size particles with self-propulsion. This is also a good approximation for at least some artificial microswimmers [12]. It has been shown that, in the absence of swimming [$\chi = 0$ in Eq. (1)], neutrally buoyant particles may detach from their corresponding fluid elements [13,14] provided that their size is sufficiently large. Therefore, a necessary condition for the validity of Eq. (1) is that such a detachment does not take place.

Interestingly, Sapsis and Haller [14] derived a rigorous condition for spherical neutrally buoyant particles to move as fluid elements. For incompressible two-dimensional fluid flows, their condition reads

$$\frac{4}{9\mathrm{St}^2} > \frac{\omega^2}{4} - \det \nabla \mathbf{u}, \tag{8}$$

where $\omega^2 = (\partial_y u_x - \partial_x u_y)^2$ is the squared vorticity and $\mathrm{St} = \frac{2}{9}(\frac{a}{L})^2\mathrm{Re}$ is the particle's Stokes number, given in terms of the particle's radius a, the characteristic length scale L of the flow, and the flow's Reynolds number Re. For the specific flow field defined by Eq. (5), it suffices to consider swimmers satisfying $\mathrm{St} < 1.7 \times 10^{-2}$ for Eq. (1) to be a good effective model in the sense discussed above.

It is worth noting that natural swimmers usually exhibit run-and-tumble motions which are not accounted for by our model. These motions can be addressed phenomenologically as a stochastic term. For instance, Doussal *et al.* model run-and-tumble motion on an infinite line using dichotomous telegraphic noise [15]. On the other hand, the analytical tools we use in Sec. IV rely on the (deterministic) Melnikov function that allows characterizing the transport across broken separatrices. Remarkably, a stochastic version of this function has been recently applied [16] to address this type of transport under colored noise. It is an interesting perspective of the present work to combine the ideas and techniques developed in [15] and [16] to increment the model studied herein.

Thermal fluctuations are also not addressed by the model studied in this paper. In the context of deformable microswimmers in a vortical fluid flow, the effects of these fluctuations have been studied by Tarama and collaborators [17]. These authors add white Gaussian noise to the equation for the time evolution of the self-propulsion velocity of the particles. They report on a threshold noise intensity below which the phenomena of capture or scattering of the swimmers by the vortex as described by the deterministic dynamics they consider remain robust. For their specific setup, that threshold noise intensity corresponds to swimmers of size close to 1 mm. Rather than using an equation of motion for the time evolution of the self-propulsion velocity, the model considered here *postulates* a self-propulsion velocity itself [cf. Eqs. (1)–(3)]. Therefore, a possible way to incorporate thermal fluctuations in our model would be to add a stochastic term generated by an Ornstein-Uhlenbeck process to the right-hand side of Eqs. (1), (2), and (3). This extension is left for future work.

Another limitation of Eq. (1) is that it does not account for the orientational dynamics of the swimmers, which should be reflected in more realistic models. We have ongoing work in which we use Jeffery's equation [18] to describe the evolution of the swimmer's orientation. Results along this line will be published elsewhere.

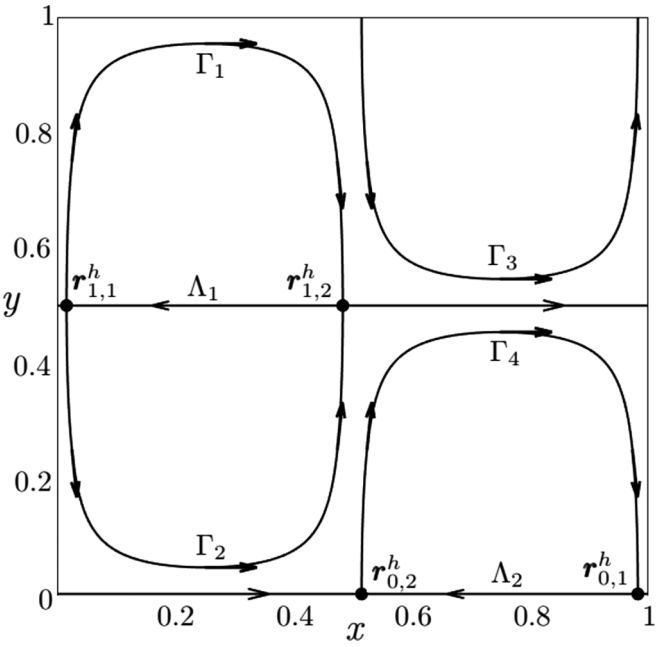

FIG. 3. Heteroclinic connections for Eq. (6) with $\epsilon = 0$ and $\alpha = \frac{\pi}{5}$. The separatrices Γ_1, Γ_2, and Λ_1 correspond to $m = 1$. The separatrices Γ_3, Γ_4, and Λ_2 correspond to $m = 0$.

III. FIRST SWIMMING STRATEGY: SELF-PROPULSION WITH CONSTANT VELOCITY

In this section we study Eq. (6) with $\epsilon = 0$, which corresponds to our first swimming strategy. This system has heteroclinic trajectories and both elliptical and hyperbolic equilibria. The equilibria of the system corresponding to the first strategy are the singular points of the vector field

$$\mathbf{X}(x, y) = \left(\frac{\partial \psi_0}{\partial y}, -\frac{\partial \psi_0}{\partial x}\right) \tag{9}$$

and can be calculated analytically. Because of the spatial periodicity of the solutions, it suffices to study the system in the square $Q \equiv [0, 1) \times [0, 1)$, where there are four hyperbolic equilibria given by

$$\mathbf{r}^h_{m,j} = \left(x^h_{m,j}, y^h_{m,j}\right) = \left(\left\{\frac{1}{4} + (-1)^j\left[\frac{1}{4} - \frac{1}{2\pi}\arcsin\left(-\frac{\alpha(-1)^m}{2\pi}\right)\right]\right\} \bmod 1, \frac{m}{2}\right), \tag{10}$$

with $m = 0$ or 1 and $j = 1$ or 2. These hyperbolic equilibria are shown in Fig. 3.

The heteroclinic connections satisfy

$$\psi_0(x, y) = \psi_0\left(x^h_{m,j}, y^h_{m,j}\right). \tag{11}$$

They are therefore given by

$$\sin(2\pi x)\sin(2\pi y) + \alpha y = \sin\left(2\pi x^h_{m,j}\right)\sin\left(2\pi y^h_{m,j}\right) + \alpha y^h_{m,j} = \frac{\alpha m}{2}, \tag{12}$$

and can be seen in Fig. 3.

As stated before, our goal is to determine which of the two strategies considered promotes more transport of the swimmers in the following sense: we aim to calculate the area of the set of initial conditions of nonconfined trajectories for each of the strategies and check which strategy leads to the largest area. This area will be equal to 1 (total area of Q) minus the area of the set of confined trajectories. For the first strategy, the latter is, due to symmetry, simply four times the area between the separatrices Γ_1 and Λ_1 shown in Fig. 3.

The equations for separatrices Γ_1 and Λ_1 are given by

$$\Gamma_1: \ \sin(2\pi x)\sin(2\pi y) + \alpha y = \frac{\alpha}{2}, \qquad 0.5 < y < 1;$$
$$\Lambda_1: \ y = 0.5, \qquad x^h_{1,1} < x < x^h_{1,2}. \tag{13}$$

From the equation for Γ_1 we can isolate x, thereby defining two functions $x_1(y)$ and $x_2(y)$, with $0.5 < y < y_{\max}$. These functions are such that $x^h_{1,1} < x_1(y) \leqslant 0.25 \leqslant x_2(y) < x^h_{1,2}$ and $x_1(y) + x_2(y) = 0.5$. The area of the region bounded by Γ_1 and Λ_1 is then given by

$$A_{\Gamma_1\Lambda_1}(\alpha) = \int_{0.5}^{y_{\max}} [x_2(y) - x_1(y)]dy, \tag{14}$$

where $y_{\max}$, $x_1(y)$, and $x_2(y)$ depend on α. In order to calculate $y_{\max}$, we note that it corresponds to the y coordinate of the intersection of Γ_1 with the straight line $x = 0.25$. In other words, $y_{\max}$ satisfies the inequality $0.5 < y_{\max} < 1$ and the transcendental equation

$$\sin(2\pi y_{\max}) + \alpha y_{\max} = \frac{\alpha}{2}. \tag{15}$$

We thus obtain the area of the set of initial conditions of confined trajectories for the first strategy:

$$A^c_1(\alpha) = 4A_{\Gamma_1\Lambda_1}(\alpha). \tag{16}$$

Finally, the area of the set of initial conditions of *escaping* (i.e., nonconfined) trajectories is

$$A^e_1(\alpha) = 1 - A^c_1(\alpha). \tag{17}$$

IV. SECOND SWIMMING STRATEGY: SELF-PROPULSION WITH PERIODIC TEMPORAL MODULATION

In this section, we characterize the transport of swimmers for the system corresponding to the second strategy, i.e., Eq. (6) with finite ϵ. The resulting dynamics is Hamiltonian, with an effective stream function given by

$$\psi_1(x, y, t) = \psi_0(x, y) + \epsilon\hat{\psi}(x, y, t), \tag{18}$$

where

$$\hat{\psi}(x, y, t) = \sin(\Omega t)y \tag{19}$$

is called a Hamiltonian perturbation and (18) is a Hamiltonian of one and a half degree of freedom.

A. The stochastic layer

The separatrices shown in Fig. 3 correspond to coinciding branches of stable and unstable manifolds of different hyperbolic fixed points. For finite ϵ, these branches no longer coincide and typically form a complex structure in phase space, called the heteroclinic tangle, in the region formerly occupied by the separatrices. This is usually accompanied by the loss of integrability of nearby orbits, which wander in a bounded region (provided that ϵ is small) called the *stochastic layer*.

The mechanism by which the stochastic layer fosters transport is related to the complex geometry of the heteroclinic tangles and can be characterized in terms of the formation of *lobes*, which are sets bounded by a segment of each of the invariant manifolds. Since the pioneering work of Rom-Kedar and collaborators [19,20], powerful techniques have been developed which use Melnikov approaches to compute the transport with great accuracy (see [21], and references therein). In particular, the *flux* across a time-evolving pseudoseparatrix can be defined and properly quantifies transport in steady two-dimensional flows under a time-periodic perturbation as well as in flows under more general time dependence (cf. Secs. 3.2–3.4 of [21]). In what follows, we use a simpler approach based on classical separatrix-map techniques [22], which nevertheless leads to reasonably accurate predictions for the gain in probability of escaping, as we report in Sec. V.

B. The separatrix map

In general, the so-called separatrix map describes the dynamics near the separatrices when an integrable system is perturbed. Weiss and Knobloch used the separatrix map to analyze transport in a binary-fluid mixture due to traveling waves [23]. It is worth noting that our unperturbed system, Eq. (6) with $\epsilon = 0$, is the same one considered in their work.

The separatrix map is obtained by considering successive intersections, to be denoted (x_n, y_n), of the trajectories of the system corresponding to the second swimming strategy with a unidimensional surface Σ fixed in the phase space. Although the map is insensitive to the specific choice of the surface, let us follow [23] and consider for concreteness any of the surfaces (where both x and y are taken modulo 1)

$$\Sigma = \Sigma^{\pm}_{m,j} = \left\{(x, y)|y = y^h_{m,j} \pm \left|x - x^h_{m,j}\right|\right\} \tag{20}$$

in a small neighborhood of the hyperbolic equilibrium $(x^h_{m,j}, y^h_{m,j})$. At each intersection (x_n, y_n), the value of the stream function corresponding to the first strategy is calculated, i.e., we define $\psi^n_0 = \psi_0(x_n, y_n)$. The other variable used in the separatrix map is the time t_n at which the trajectory crosses the line x modulo $1 = 0.75 - m/2$ with positive $\dot{x}$ just prior to the $(n+1)$th intersection with $\Sigma^{\pm}_{m,j}$. Note that, defining s_n by $(x_n, y_n) = [x(s_n), y(s_n)]$, we have $t_n < s_{n+1} < t_{n+1}$.

Provided that ϵ is sufficiently small, the rate of change of ψ_0 along an actual trajectory of Eq. (6) can be approximated by the corresponding rate along the separatrix. If we also use the approximation $t_{n+1} - t_n \simeq T(\psi^{n+1}_0)$, where $T(h)$ is the period of the stream function $\psi_0 = h$, we obtain the separatrix map as [22,23]

$$\begin{aligned} \psi^{n+1}_0 &= \psi^n_0 + \epsilon M(t_n), \\ t_{n+1} &= t_n + T\left(\psi^{n+1}_0\right), \end{aligned} \tag{21}$$

where M is the Melnikov function calculated in Appendix A.

C. Boundary of the stochastic layer

We obtain an approximation for the period $T(\psi_0^{n+1})$ in Appendix B. Using that result, the separatrix map (21) reads

$$\psi_0^{n+1} = \psi_0^n + \epsilon M(t_n),$$
$$t_{n+1} = t_n + (-1)^{(m+j+1)}\left(\frac{2}{k}\right)\ln\left|\frac{2\psi_0^{n+1} - \alpha m}{2k\left(x_0 - x_{m,j}^h\right)\left(y_1 - y_{m,j}^h\right)}\right|, \tag{22}$$

where k is given by Eq. (B6) and x_0 and y_1 are also defined in Appendix B (see the caption of Fig. 6). To obtain the curve separating confined trajectories of nonconfined ones, we first use the criterion given in [22] to locate the boundaries of the stochastic layer,

$$\max_{t_n}\left|\frac{\partial t_{n+1}}{\partial t_n} - 1\right| = 1, \tag{23}$$

which corresponds to the observation that the dynamical instability associated to separatrix chaos first manifests itself as the stretching of the variable t_n. Using Eq. (22), we obtain

$$\max_{t_n}\left|\frac{\partial t_{n+1}}{\partial t_n} - 1\right| = \left|\frac{4\epsilon}{k\left(2\psi_0^{n+1} - \alpha m\right)}\right|\max_{t_n}\left|\frac{dM}{dt_n}\right|. \tag{24}$$

From the expression for the Melnikov function given in (A4), we get

$$\begin{aligned}\max_{t_n}\left|\frac{dM}{dt_n}\right| &= \max_{t_n}\left|2\pi\,\Omega I_i(\alpha,\Omega)\sin(\Omega t_n)\right| \\ &= 2\pi\,\Omega|I_i(\alpha,\Omega)|,\end{aligned} \tag{25}$$

where $I_i(\alpha,\Omega)$ is defined by Eq. (A5). Using Eqs. (24) and (25), Eq. (23) becomes

$$\left|\frac{8\epsilon\pi\,\Omega I_i(\alpha,\Omega)}{k(2\psi_0^{n+1} - \alpha m)}\right| = 1. \tag{26}$$

The above equality describes the following curves which form the boundary of the stochastic layer:

$$\begin{aligned}\psi_0(x,y) = \psi_0^{s_1} &\equiv \frac{\alpha m}{2} + \frac{2\epsilon\Omega I_i(\alpha,\Omega)}{\sqrt{4\pi^2 - \alpha^2}}, \\ \psi_0(x,y) = \psi_0^{s_2} &\equiv \frac{\alpha m}{2} - \frac{2\epsilon\Omega I_i(\alpha,\Omega)}{\sqrt{4\pi^2 - \alpha^2}}.\end{aligned} \tag{27}$$

D. Measure of the set of initial conditions of escaping solutions

We now observe that, for each separatrix Γ_i, one of the above curves is located in the region of escaping trajectories of the unperturbed system whereas the other one lies in the region of confined trajectories. The latter will, in the *perturbed* system (i.e., the one corresponding to the second swimming strategy), separate escaping from confined solutions since chaos breaks transport barriers.

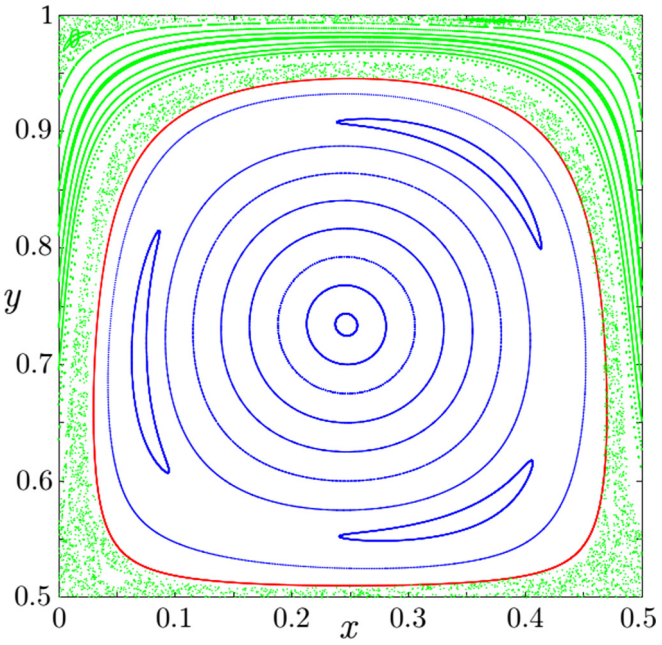

FIG. 4. Theoretical boundary (red), predicted by Eq. (28), between the regions of confined (blue) and escaping (green) solutions. The parameters are $\alpha = \pi/5$, $\epsilon = 0.2$, and $\Omega = 80$.

The region corresponding to confined trajectories is therefore contained by one of the following curves:

$$\sin(2\pi x)\sin(2\pi y) + \alpha y = \psi_0^s = \begin{cases}\dfrac{\alpha m}{2} + \dfrac{2\epsilon\Omega I_i(\alpha,\Omega)}{\sqrt{4\pi^2 - \alpha^2}} \\ \text{or} \\ \dfrac{\alpha m}{2} - \dfrac{2\epsilon\Omega I_i(\alpha,\Omega)}{\sqrt{4\pi^2 - \alpha^2}}.\end{cases} \tag{28}$$

Let $\zeta = \psi_0^{-1}(\psi_0^s)$ be such a curve, depicted for a specific choice of parameters in Fig. 4. In order to calculate the area A_ζ enclosed by ζ, we proceed as in Sec. II. We obtain

$$A_\zeta = \int_{y_{\min}}^{y_{\max}}[x_2(y) - x_1(y)]dy, \tag{29}$$

where x_2 and x_1 are the functions of y implicitly defined by ζ, and $y_{\min}$ and $y_{\max}$ are the two solutions of

$$\sin(2\pi y) + \alpha y = \psi_0^s$$

and

$$-\sin(2\pi y) + \alpha y = \psi_0^s,$$

respectively, for $i \leqslant 2$ and $i \geqslant 3$.

Then, the area of the set of initial conditions of confined trajectories within the unit square is given by

$$A_2^c = 4A_\zeta \tag{30}$$

and the area of the set of initial conditions of nonconfined trajectories within the unit square is

$$A_2^e = 1 - A_2^c. \tag{31}$$

We note that A_2^e is a function of α, ϵ, and Ω.

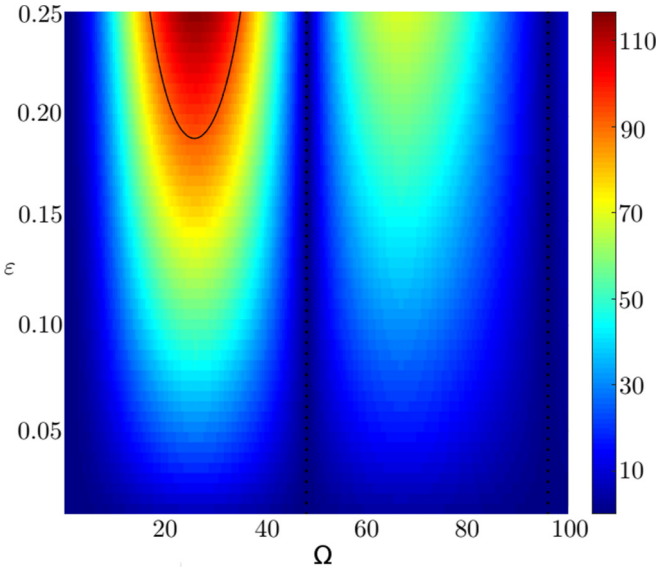

FIG. 5. Percentage increase of the area of the set of initial conditions of nonconfined trajectories for the second swimming strategy as compared to the corresponding area for the first swimming strategy. The other parameter is $\alpha = \frac{\pi}{5}$. The region under the black curve is the validity region, where the parameters satisfy inequality (32). The two vertical dashed lines correspond to the values of Ω for which the Melnikov function vanishes.

V. COMPARISON BETWEEN THE SWIMMING STRATEGIES

We have used our theoretical results, Eqs. (17) and (31), to compare the two strategies for different values of the parameters α, ϵ, and Ω. In Fig. 5, the percentage variation of the area of the set of initial conditions of nonconfined trajectories is shown as a function of ϵ and Ω for a fixed value of α. Note the existence of values of the parameters for which the percentage increase exceeds 80%.

To validate our analytical results, we have also calculated, for specific values of the parameters, the same quantities using numerical methods. For that purpose, we have chosen initial conditions near the separatrices Γ_1, Γ_2, Γ_3, and Γ_4 until obtaining the four curves separating confined from nonconfined motion. This was performed numerically by means of the bisection method, with an error smaller than 10^{-6}. We have used the bubble sort algorithm [24] to index each point of these curves and, from that, obtained the area of the region within each such curve using numerical integration. Finally, by adding the area of the four regions, we have computed the area of the set of initial conditions of confined trajectories in the square Q. Numerical results (not shown) indicate good agreement with our analytical predictions (deviations not larger than 5%) for most of the parameter range depicted in Fig. 5.

Deviations are, however, expected in two cases. First, close to the two vertical dashed lines shown in the figure, where the Melnikov function vanishes and analysis up to second order is necessary, which is beyond the scope of the present work. Second, as the parameters approach the region above the black curve in the uppermost left part of the figure, where the following inequality does not hold:

$$8\Omega\epsilon|I_i(\alpha, \Omega)| \leqslant \alpha\sqrt{4\pi^2 - \alpha^2}. \tag{32}$$

This is a condition for the validity of our analytical results for the second strategy. It arises because, if the perturbation ϵ is large enough, the exterior boundary curve of the stochastic region close to Γ_1 (respectively, Γ_2) collides with the exterior boundary curve of the stochastic region close to Γ_3 (respectively, Γ_4).

Given the recent advances in experimental techniques to investigate chaotic structures in two-dimensional flows (see, e.g., [25]), it seems reasonable to assume that an experimental assessment of the chaotic behavior of the swimmers might be already feasible if the relative area of the stochastic layer is of the order of 1% or larger. As a rule of thumb for the the parameter region depicted in Fig. 5, this occurs if $\epsilon \gtrapprox 0.02$ provided that one is not too close to the resonant frequencies where the Melnikov function vanishes (vertical dashed lines in Fig. 5).

VI. CONCLUSIONS

We have compared two strategies of swimming particles. The systems corresponding to these strategies display both confined and escaping trajectories, and our goal here was to determine which strategy leads to a larger probability of escaping. For the first strategy the calculations are easier since it corresponds to an integrable system. The second strategy is a periodic perturbation of the first one. Using separatrix-map techniques we could approximate analytically the boundary of the region of escaping solutions. This has allowed us to show that the area of initial conditions leading to nonconfined trajectories increases as we replace the first by the second strategy. Our main result is the analytical quantification of that increase.

Research started in this work suggests some interesting extensions. First, new bases of comparison between strategies that take into account not only the area of the set of initial conditions leading to nonconfined trajectories but also the average velocity of the swimmers may be introduced and exploited. Second, it would be interesting to investigate new strategies for swimmers that can obtain local information about the flow (e.g., pressure gradients). It would also be interesting to compare all these strategies with the optimal strategy, which can be obtained by means of variational methods and requires global knowledge of the flow.

Finally, an important perspective of the present work is the consideration of a nonphenomenological equation of motion for specific types of phototactic swimmers. Such an equation must at some point account for their finite size. Finite-sizeness is known to render the dynamics dissipative [13,26–28], which may lead to the formation of attractors where particles accumulate, a phenomenon which was addressed for heavy finite-size particles in [29,30].

ACKNOWLEDGMENTS

The authors are grateful to J.-R. Angilella for illuminating discussions and the anonymous referees for important sug-

gestions. A.J.G. was supported by a Ph.D. fellowship from CAPES.

APPENDIX A: MELNIKOV FUNCTIONS

In general, if $\boldsymbol{\gamma}_i(t) = [x_i(t), y_i(t)]$ is a parametrization of the separatrix Γ_i, where $i = 1,\ 2,\ 3,$ or 4, the corresponding Melnikov function is defined by

$$M_i(\theta_0) = \int_{-\infty}^{+\infty} \{\psi_0[\boldsymbol{\gamma}_i(t-\theta_0)], \hat{\psi}[\boldsymbol{\gamma}_i(t-\theta_0), t]\}dt, \quad \text{(A1)}$$

where

$$\{\psi_0, \hat{\psi}\} = \frac{\partial\psi_0}{\partial x}\frac{\partial\hat{\psi}}{\partial y} - \frac{\partial\psi_0}{\partial y}\frac{\partial\hat{\psi}}{\partial x} \quad \text{(A2)}$$

is the *Poisson bracket* of ψ_0 with $\hat{\psi}$.

The meaning of the Melnikov function is the following: $\epsilon M_i(\theta)$ is proportional to the *signed* distance, to first order in ϵ, between stable and unstable manifolds which replace Γ_i when $\epsilon = 0$ is replaced by a small but finite ϵ in Eq. (6).

Replacing Eqs. (7), (19), and (A2) in Eq. (A1), we obtain the following expression for the Melnikov function:

$$M_i(\theta_0) = \int_{-\infty}^{+\infty} 2\pi\cos[2\pi x_i(t-\theta_0)]\sin[2\pi y_i(t-\theta_0)]\sin(\Omega t)dt, \quad \text{(A3)}$$

where, for the sake of simplicity, the dependence of M_i on the parameters α (since both x_i and y_i depend on α) and Ω has not been made explicit in the notation. After the substitution $t \mapsto t - \theta_0$, the Melnikov function reads

$$\begin{aligned} M_i(\theta_0) &= \int_{-\infty}^{+\infty} 2\pi\cos[2\pi x_i(t)]\sin[2\pi y_i(t)]\sin[\Omega(t+\theta_0)]dt \\ &= 2\pi[I_i(\alpha,\Omega)\cos(\Omega\theta_0) + J_i(\alpha,\Omega)\sin(\Omega\theta_0)], \end{aligned} \quad \text{(A4)}$$

where

$$I_i(\alpha,\Omega) = \int_{-\infty}^{+\infty} \cos[2\pi x_i(t)]\sin\lceil 2\pi y_i(t)\rceil\sin(\Omega t)dt \quad \text{(A5)}$$

and

$$J_i(\alpha,\Omega) = \int_{-\infty}^{+\infty} \cos[2\pi x_i(t)]\sin[2\pi y_i(t)]\cos(\Omega t)dt. \quad \text{(A6)}$$

By means of a suitable choice of the initial condition $\boldsymbol{\gamma}_i(0)$ for each Γ_i, we can simplify the above integrals. In particular, we choose $\boldsymbol{\gamma}_1(0)$ and $\boldsymbol{\gamma}_2(0)$ as the intersections of the straight line $x = 0.25$ with Γ_1 and Γ_2, respectively. Analogously, we choose $\boldsymbol{\gamma}_3(0)$ and $\boldsymbol{\gamma}_4(0)$ as the intersections of the straight line $x = 0.75$ with Γ_3 and Γ_4, respectively. We then obtain

$$I_i(\alpha,\Omega) = 2\int_0^{+\infty} \cos[2\pi x_i(t)]\sin[2\pi y_i(t)]\sin(\Omega t)dt$$

and

$$J_i(\alpha,\Omega) = 0$$

for all positive α and Ω. We also obtain $I_1 = I_4 = -I_2 = -I_3$.

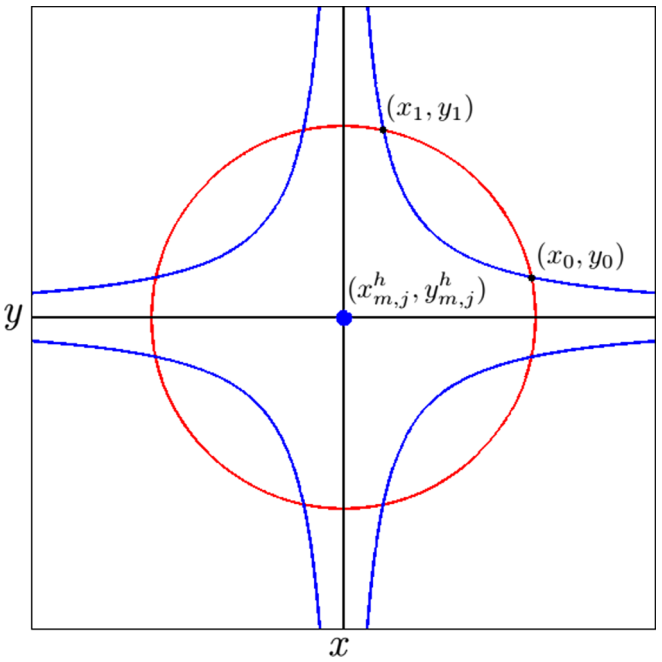

FIG. 6. Solutions of Eq. (B7) (blue) in the neighborhood of a hyperbolic equilibrium $(x^h_{m,j}, y^h_{m,j})$. The intersection points of one such solution with the boundary (in red) of an open ball centered at the equilibrium are (x_0, y_0) and (x_1, y_1), where the former is visited before the latter. In black, we show the stable and unstable spaces of $(x^h_{m,j}, y^h_{m,j})$.

Melnikov functions are similarly defined for the horizontal separatrices shown in Fig. 3, as for example Λ_1. Because of the parametrizations of these separatrices, however, the corresponding Melnikov functions vanish identically. This is consistent with the survival of the horizontal separatrices when ϵ is switched from zero to a finite value in Eq. (6).

APPENDIX B: APPROXIMATE EXPRESSION FOR $T(\psi_0^{n+1})$

We now turn to the second equation (21). The problem to be dealt with is that there is no analytical representation for $T(\psi_0^{n+1})$. However, the dynamics of the trajectories in the neighborhood of an equilibrium is very slow, meaning that we can use a Taylor expansion of ψ_0 in the neighborhood of a hyperbolic equilibrium of the system corresponding to the first strategy to approximate $T(\psi_0^{n+1})$ [31,32].

The Taylor expansion for ψ_0 in a neighborhood of a hyperbolic equilibrium $(x^h_{m,j}, y^h_{m,j})$ is given by

$$\begin{aligned} &\psi_0\left(x^h_{m,j}+u, y^h_{m,j}+v\right) \\ &\quad\approx \psi_0\left(x^h_{m,j}, y^h_{m,j}\right) + \tfrac{1}{2}[u\ v]\nabla^2\psi_0\left(x^h_{m,j}, y^h_{m,j}\right)[u\ v]^t, \end{aligned} \quad \text{(B1)}$$

where the matrix $\nabla^2\psi_0(x^h_{m,j}, y^h_{m,j})$ is given by

$$\nabla^2\psi_0\left(x^h_{m,j}, y^h_{m,j}\right) = (-1)^{(m)}4\pi^2\begin{bmatrix} 0 & \cos\left(2\pi x^h_{m,j}\right) \\ \cos\left(2\pi x^h_{m,j}\right) & 0 \end{bmatrix}. \quad \text{(B2)}$$

Using Eq. (10), we obtain

$$\cos\left(2\pi x^h_{m,j}\right) = (-1)^{j+1}\frac{\sqrt{4\pi^2-\alpha^2}}{2\pi}. \tag{B3}$$

Thus, the matrix in Eq. (B2) is

$$\nabla^2\psi_0\left(x^h_{m,j}, y^h_{m,j}\right) = (-1)^{(m+j+1)}2\pi\sqrt{4\pi^2-\alpha^2}\begin{bmatrix}0 & 1\\ 1 & 0\end{bmatrix}. \tag{B4}$$

Using the above equality and Eq. (12), we can recast (B1) as

$$\psi_0(x,y) \approx \frac{\alpha m}{2} + (-1)^{(m+j+1)}k\left(x - x^h_{m,j}\right)\left(y - y^h_{m,j}\right), \tag{B5}$$

where

$$k = 2\pi\sqrt{4\pi^2-\alpha^2}, \tag{B6}$$

from which the approximated equations for the trajectories in a neighborhood of $(x^h_{m,j}, y^h_{m,j})$ are derived:

$$\begin{aligned}\frac{dx}{dt} &= (-1)^{(m+j+1)}k\left(x - x^h_{m,j}\right),\\ \frac{dy}{dt} &= (-1)^{(m+j)}k\left(y - y^h_{m,j}\right).\end{aligned} \tag{B7}$$

Noting that the trajectory on the streamline $\psi_0 = H$ close to a separatrix spends a time interval roughly given by $T(\psi_0)/2$ in the neighborhood of each hyperbolic equilibrium it approaches, we can integrate the first equation (B7) to write

$$\ln\left|\frac{x_1 - x^h_{m,j}}{x_0 - x^h_{m,j}}\right| = (-1)^{(m+j+1)}T(H)\frac{k}{2}, \tag{B8}$$

where (x_0, y_0) and (x_1, y_1) are the points where a solution of (B7) intersects the boundary of an open ball centered at the hyperbolic equilibrium $(x^h_{m,j}, y^h_{m,j})$, as shown in Fig. 6. Using Eq. (B5) to compute $H = \psi_0(x_1, y_1)$, we can express $x_1 - x^h_{m,j}$ in terms of H. Equation (B8) then becomes

$$T(H) = (-1)^{(m+j+1)}\frac{2}{k}\ln\left|\frac{2H - \alpha m}{2k\left(x_0 - x^h_{m,j}\right)\left(y_1 - y^h_{m,j}\right)}\right|. \tag{B9}$$

[1] Z. Neufeld and E. Hernandez-Garcia, *Chemical and Biological Processes in Fluid Flows: A Dynamical Systems Approach* (Imperial College Press, London, 2010).
[2] A. Giometto, F. Altermatt, A. Maritan, R. Stocker, and A. Rinaldo, Proc. Natl. Acad. Sci. USA **112**, 7045 (2015).
[3] J. Arrieta, A. Barreira, M. Chioccioli, M. Polin, and I. Tuval, Sci. Rep. **7**, 3447 (2017).
[4] B. Dai, J. Wang, Z. Xiong, X. Zhan, W. Dai, C.-C. Li, S.-P. Feng, and J. Tang, Nat. Nanotechnol. **11**, 1087 (2016).
[5] C. Lozano, B. ten Hagen, H. Löwen, and C. Bechinger, Nat. Commun. **7**, 12828 (2016).
[6] C. Torney and Z. Neufeld, Phys. Rev. Lett. **101**, 078105 (2008).
[7] X. Garcia, S. Rafaï, and P. Peyla, Phys. Rev. Lett. **110**, 138106 (2013).
[8] J. S. Guasto, K. A. Johnson, and J. P. Gollub, Phys. Rev. Lett. **105**, 168102 (2010).
[9] R. Chacón, Phys. Rev. E **88**, 052905 (2013).
[10] A. M. Ardekani and E. Gore, Phys. Rev. E **85**, 056309 (2012).
[11] S. Yazdi and A. M. Ardekani, Biomicrofluidics **6**, 044114 (2012).
[12] A. Acemoglu and S. Yesilyurt, Microfluid Nanofluid **19**, 1109 (2015).
[13] A. Babiano, J. H. E. Cartwright, O. Piro, and A. Provenzale, Phys. Rev. Lett. **84**, 5764 (2000).
[14] T. Sapsis and G. Haller, Phys. Fluids **20**, 017102 (2008).
[15] P. Le Doussal, S. N. Majumdar, and G. Schehr, Phys. Rev. E **100**, 012113 (2019).
[16] J.-R. Angilella, Phys. Rev. E **99**, 032224 (2019).
[17] M. Tarama, A. M. Menzel, and H. Löwen, Phys. Rev. E **90**, 032907 (2014).
[18] G. B. Jeffery, Proc. R. Soc. A **102**, 161 (1922).
[19] V. Rom-Kedar, A. Leonard, and S. Wiggins, J. Fluid Mech. **214**, 347 (1990).
[20] S. Wiggins, *Chaotic Transport in Dynamical Systems* (Springer-Verlag, New York, 1992).
[21] S. Balasuriya, *Barriers and Transport in Unsteady Flows* (SIAM, Philadelphia, 2016).
[22] G. M. Zaslavsky, *The Physics of Chaos in Hamiltonian Systems*, 2nd ed. (Imperial College Press, London, 2007).
[23] J. B. Weiss and E. Knobloch, Phys. Rev. A **40**, 2579 (1989).
[24] T. H. Cormen, C. E. Leiserson, R. L. Rivest, and C. Stein, *Introduction to Algorithms* (MIT Press, Cambridge, MA, 2009).
[25] P. Meunier, P. Huck, C. Nobili, and E. Villermaux, Phys. Fluids **27**, 077103 (2015).
[26] R. D. Vilela, A. P. S. de Moura, and C. Grebogi, Phys. Rev. E **73**, 026302 (2006).
[27] J. H. E. Cartwright, U. Feudel, G. Károlyi, A. de Moura, O. Piro, and T. Tél, Dynamics of finite-size particles in chaotic fluid flows, in *Nonlinear Dynamics and Chaos: Advances and Perspectives. Understanding Complex Systems*, edited by M. Thiel, J. Kurths, M. Romano, G. Károlyi, and A. Moura (Springer, Berlin, Heidelberg, 2010).
[28] R. D. Vilela and V. M. de Oliveira, Eur. Phys. J.: Spec. Top. **226**, 2079 (2017).
[29] R. D. Vilela and A. E. Motter, Phys. Rev. Lett. **99**, 264101 (2007).
[30] J.-R. Angilella, R. D. Vilela, and A. E. Motter, J. Fluid Mech. **744**, 183 (2014).
[31] L. Kuznetsov and G. M. Zaslavsky, Phys. Rev. E **58**, 7330 (1998).
[32] J.-R. Angilella, Phys. Fluids **23**, 113602 (2011).